Proceedings of DETC'02
ASME 2002 Design Engineering Technical Conferences and Computers and Information in Engineering Conference
Montreal, Canada, September 29-October 2, 2002

DETC2002/MECH-34287

ON THE DESIGN OF A LOW - FORCE 5 - DOF FORCE - FEEDBACK HAPTIC MECHANISM

Evangelos Papadopoulos
Department of Mechanical Engineering,
National Technical University of Athens,
15780 Athens, Greece
egpapado@central.ntua.gr

Kostas Vlachos
Department of Mechanical Engineering,
National Technical University of Athens,
15780 Athens, Greece
kostaswl@central.ntua.gr

Dionyssios Mitropoulos
School of Medicine,
National Capodistrian University of Athens,
115 27 Athens, Greece
dmp@otenet.gr

ABSTRACT

Virtual reality is becoming very important for training medical surgeons in various operations. Interfacing users with a virtual training environment, requires the existence of a properly designed haptic device. This paper presents the design of a new force feedback haptic mechanism with five active degrees of freedom (dof), which is used as part of a training simulator for urological operations. The mechanism consists of a two dof, 5–bar linkage and a three dof spherical joint, designed to present low friction, inertia and mass, to be statically balanced, and have a simple mass matrix. The device is suitable for the accurate application of small forces and moments. All five actuators of the haptic device are base-mounted DC motors and use a force transmission system based on capstan drives, pulleys and miniropes. The paper describes the chosen design, and its kinematics, dynamics, and control algorithm and hardware employed.

INTRODUCTION

During the past several years, research on the use of virtual reality in medicine has rapidly increased. Because of the recent development in software and hardware, it is now possible to create realistic simulation environments for educational purposes in medicine, [1]. Training in a simulated environment has significant advantages against the traditional medical training. It is a less expensive and results in a faster way for training and practice in complicated procedures, [2]. The practice on animals becomes an undesired alternative for ethical and economical reasons. Also, the existence of a training simulator yields greater availability of the training environment and allows an easier evaluation of the performance of the trainee.

Development of a useful and sufficiently realistic surgical simulator requires the use of two core technologies such as of graphical simulation in a virtual reality context and of haptic technologies including force feedback. While a realistic visual representation of human anatomy and tissue deformation are very important, the ability to command the graphic environment and interact with it through the feel of the forces and torques is also of paramount importance. In order to implement such a feel, haptic devices are used.

The earliest haptic devices were of the master – slave type, and were used for telemanipulation of hazardous materials, [3]. In the last fifteen years, the availability of powerful computers, have resulted in the proliferation of virtual reality systems. In these systems, the slave has been replaced by a computational model and its motion appears graphically.

Today, one can distinguish two trends in the development of medical simulators. The first is described by the use of general-purpose haptic devices, like the Phantom or the Freedom – 7, [4, 5, 6]. The Phantom is a five bar parallel mechanism with three or six degrees-of-freedom (dof) which is designed as a general-use haptic interface, [7]. The Phantom 1.5/6DOF and the Phantom Premium 6DOF Prototype have six active dof, but are designed mainly for virtual prototyping,

virtual assembly, etc. The actuators are mounted on the moving parts of the mechanism, the mechanism inertia is relative large, and the acting forces and workspace are not suitable for the operation described in this paper, [8]. A training simulator for the diagnosis of prostate cancer using the Phantom haptic interface is described in [9]. Freedom – 7 is a haptic device with six dof for translation and rotation plus a seventh for the movement of tools like scissors and forceps. It has six active dof and is also designed for general haptic applications, [10].

The second trend is described by the use of haptic devices designed for a specific operation. The PantoScope belongs to this category. It is a four dof mechanism for force reflection in a laparoscopic surgery simulation environment, [11]. The Laparoscopic Impulse Engine is another haptic device for laparoscopic and endoscopic procedures with five dof of which three provide force feedback. VIRGY is an endoscopic surgery simulator, which uses the PantoScope haptic device, [12]. The "Karlsruhe Endoscopic Surgery Trainer" and the "Virtual Endoscopic Surgery Training" (VEST) are training simulators specialized in laparoscopic operations using the software system KISMET, [13]. Three types of force reflecting interfaces can be connected to KISMET, the Laparoscopic Impulse Engine, the Phantom and the HIT Force Feedback Device designed in Forschungszentrum Karlsruhe. All these force feedback devices have three active dof only.

This paper presents a new five dof haptic device for training in male urological operations, of which all five dof are active. The mechanism allows three dof tool orientation motions and two dof translation motions. The orientation pitch-roll-yaw dof are decoupled from themselves and from the mechanism translational dof. Unlike other haptic devices in which the maximum forces or torques are of prime importance, here it is very important to have a device that can reproduce faithfully very small forces and torques, like those that appear in urological operations. Therefore, a major effort was placed in designing the mechanism such that it is characterized by minimum friction and inertia. The paper analyzes the kinematics and the dynamics of the mechanism, and describes its mechanical design. It proposes a control law and presents implementation solutions.

NOMENCLATURE

(O, X, Y, Z)	=	reference coordinate frame
(O′, X′, Y′, Z′)	=	body – fixed coordinate frame
A_i, B_i, C_i	=	idler pulleys
$\mathbf{F}$	=	force & torque vector
$\mathbf{F}_r$	=	tissue deformation forces & torques
$\mathbf{G}$	=	gravity torques vector
$\mathbf{J}$	=	Jacobian matrix
$\mathbf{K}_{amp}$	=	amplifier gains
$\mathbf{K}_T$	=	motors torque constants
$\mathbf{M}$	=	mass matrix
$\mathbf{V}$	=	nonlinear velocity terms vector
g	=	acceleration of gravity
$\mathbf{i}$	=	vector of motor currents
l_{bi}	=	ith balancing mass offset
l_i	=	ith link length
l_{ci}	=	ith link mass center location, Fig. 3
m_i	=	ith link mass
$\mathbf{N}$	=	transmission ratio matrix
$\mathbf{q}$	=	joint angles vector
$\dot{\mathbf{q}}$	=	joint rates vector
q_i	=	ith joint angle
$q_{i,end}$	=	ith joint angle at the end of the path
$\mathbf{v}$	=	linear & angular velocities vector
x, y	=	endpoint Cartesian position
Ψ	=	angle between link 4 and endoscope
θ	=	endoscope path absolute angle
$\boldsymbol{\tau}$	=	actuator torque vector
$\boldsymbol{\tau}'$	=	joint torque vector
$\omega_x, \omega_y, \omega_z$	=	angular velocities

REQUIREMENTS

During a urological operation on a male, the surgeon has to insert a long cylindrical endoscope, see Fig. 1, until its endpoint reaches the patient's bladder. A tiny camera at the endoscope endpoint provides optical information about the endpoint location and the condition of the tissues.

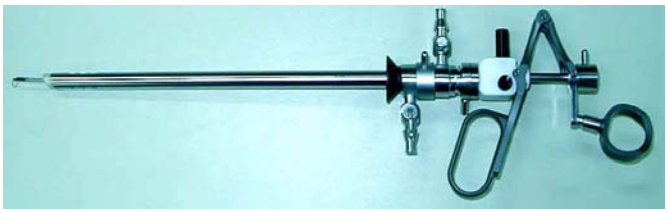

Fig. 1. Endoscope for urological operations.

Observations of actual operations on humans and animals showed that a urological operation can be divided into two phases, i.e. the insertion phase and the main operation.

During insertion, the endoscope follows a typical path as shown in Fig. 2. The surgeon moves the tip of the endoscope from the insertion point A to the final point C, via an intermediate point B, see Fig. 2. At point B, the endoscope orientation changes without translation, so as to align the entire urethra and continue the insertion phase without traumas. The corresponding endoscope configurations labeled by a, b, c, d, are shown in Fig. 2.

When the endpoint of the endoscope reaches the bladder (point C in Fig. 2), the surgeon inserts through the endoscope a mechanism with scissor-like handle and begins the second phase. This phase is the main operation in which tissue removal occurs. During this phase, the movements of the endoscope are mainly rotational.

Further, observations of actual operations showed that although the endoscope can have any orientation in a cone, its endpoint translations occur on a plane of symmetry of the

patient. Therefore, a five-dof haptic mechanism is needed, with two translational and three rotational dof.

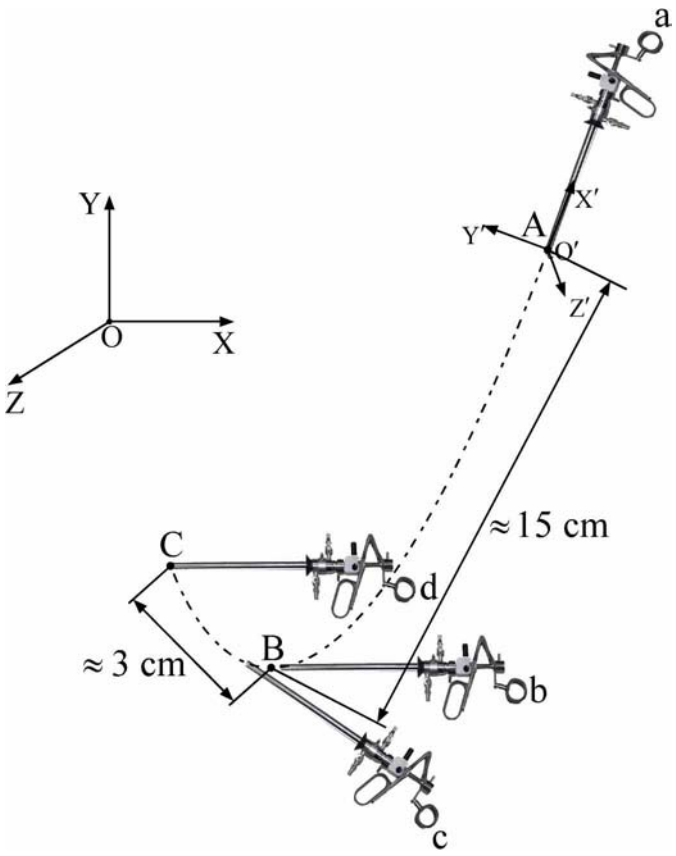

Fig. 2. Endoscope path during an operation.

The actual kinematic requirements that define the workspace of the haptic interface are shown in Table 1. These were found by actual observations of typical urological operations. The workspace is defined with respect to a reference coordinate frame (O, X, Y, Z), where O is the base point of the mechanism and X-Y the plane of symmetry of the patient. The rotations are defined with respect to an endoscope body-fixed coordinate frame (O′, X′, Y′, Z′). The translation along the endoscope path ABC in Fig. 2 is of the order of 20 cm.

Table 1. Haptic device workspace requirements.

Translation along the X axis	10 cm
Translation along the Y axis	10 cm
Translation along the Z axis	0 cm
Rotation about X′ axis	±180°
Rotation about Y′ axis	± 30°
Rotation about Z′ axis	± 30°

The forces that the surgeon feels during the operation are small but of great importance, because they provide feedback needed for the successful accomplishment of the operation. In order to reproduce these small forces the haptic mechanism must be balanced, have low inertia, low friction, no backlash and be absolutely backdriveable.

The maximum values of the endoscope-imposed forces and torques were measured in collaboration with specialist surgeons and are shown in Table 2. However, the forces and torques felt during the operation can be a fraction of these maximum values. This makes the design of a haptic device for such operations quite challenging.

Table 2. Maximum values of imposed forces and torques during a urological operation.

Force along the X axis	1.5 N
Force along the Y axis	1.5 N
Torque about the X' axis	2.0 mNm
Torque about the Y' axis	70.0 mNm
Torque about the Z' axis	70.0 mNm

KINEMATICS & DYNAMICS

A hybrid design of a closed and a serial mechanism was developed that satisfies in principle the device kinematic requirements. It consists of a 5–bar parallel linkage with two translational dofs in series to a spherical joint with three rotational dofs, as depicted schematically in Fig. 3. The mechanism origin is located at the joint linking links 2 and 3 and not the joint linking links 1 and 2, see Fig. 3. This choice was dictated by the fact that the chosen configuration gives better static and dynamic behavior for the typical path in Fig. 2. The endoscope is attached at point E in Fig. 3, i.e. the point at which the three axes of the last three joints intersect. For design reasons, both the differential kinematics and the dynamics of the mechanism are important and developed next.

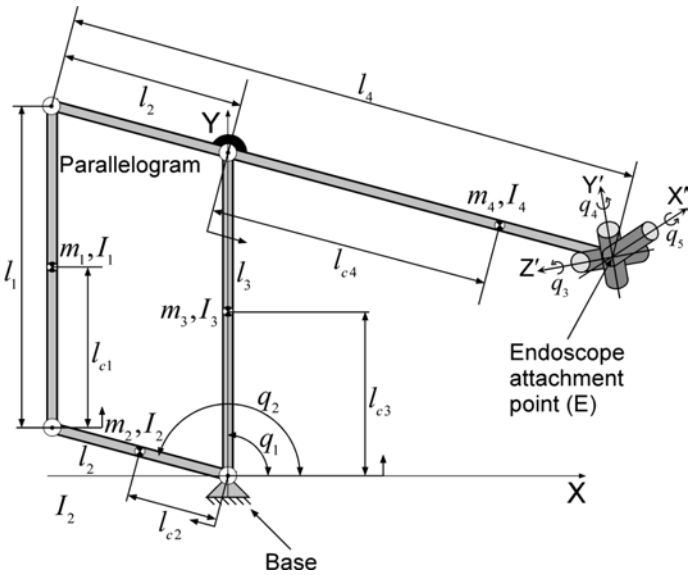

Fig. 3. Schematic view of a 5 dof haptic mechanism and its kinematic and dynamic parameters.

The differential kinematics for this mechanism relate the endpoint Cartesian velocities and angular velocities $\mathbf{v} = [\dot{x}, \dot{y}, \omega_x, \omega_y, \omega_z]^T$ to joint rates $\dot{\mathbf{q}} = [\dot{q}_1, \dot{q}_2, \dot{q}_3, \dot{q}_4, \dot{q}_5]^T$

$$\mathbf{v} = \mathbf{J}(\mathbf{q})\dot{\mathbf{q}} \tag{1}$$

The Jacobian $\mathbf{J}(\mathbf{q})$ is a 5×5 square matrix. The translational five bar mechanism becomes singular when $q_1 = q_2$ or $q_1 = q_2 \pm \pi$. The spherical joint, which is of the z-y-x type, becomes singular when $q_4 = \pm\pi/2$. However, all these configurations are not possible to the constructed mechanism due to its design. Therefore, the actual device is free of singularities in its workspace.

Employing a Lagrangian formulation yields the following mechanism equations of motion

$$\mathbf{M}(\mathbf{q})\ddot{\mathbf{q}} + \mathbf{V}(\mathbf{q},\dot{\mathbf{q}}) + \mathbf{G}(\mathbf{q}) = \boldsymbol{\tau}' + \mathbf{J}^T\mathbf{F}_T \tag{2}$$

In Eq. (2), $\mathbf{M}(\mathbf{q})$ is the mechanism 5×5 mass matrix, $\ddot{\mathbf{q}}$ is the joint accelerations vector, $\mathbf{V}(\mathbf{q},\dot{\mathbf{q}})$ is a vector which contains the nonlinear velocity terms and $\mathbf{G}(\mathbf{q})$ is the gravity torques vector. The vector $\boldsymbol{\tau}'$ contains joint input torques while the vector $\mathbf{J}^T\mathbf{F}_T$ resolves the forces and torques applied by the endoscope to the mechanism endpoint, to the five joints.

For control reasons, it is useful to eliminate the gravitational terms. Otherwise, the controller would have to provide control torques to balance the mechanism and make it transparent to the user. To this end, an accurate knowledge of the mass properties of the system is required, something difficult to achieve.

Assuming that the spherical joint center of mass coincides with the axes intersection, the nonzero gravitational static terms for the unbalanced mechanism are

$$g_1(\mathbf{q}) = g\mathrm{c}_1\left(m_1 l_{c1} + m_3 l_{c3} + (m_4 + m_5 + m_6 + m_7) l_3\right) \tag{3a}$$

$$g_2(\mathbf{q}) = g\,\mathrm{c}_2(m_1 l_2 + m_2 l_{c2} - m_4 l_{c4} - (m_5 + m_6 + m_7)(l_4 - l_2)) \tag{3b}$$

These terms can be eliminated if two balancing weights are used with masses m_{b2} and m_{b3} given by

$$\begin{aligned} m_{b3} &= (m_3 l_{c3} + (m_4 + m_5 + m_6 + m_7) l_3 - m_{c3} l_{cb3} + m_1 l_{c1}) / l_{b3} \\ m_{b2} &= (m_4 l_{c4} + (m_5 + m_6 + m_7) l_{4-2} - m_1 l_2 - m_{c2} l_{cb2} - m_2 l_{c2}) / l_{b2} \end{aligned} \tag{4}$$

where $l_{4-2} = l_4 - l_2$. The balancing weights are located on the extensions of links 2 and 3, at distances l_{b2} and l_{b3} from the base point of the mechanism respectively. These lengths were chosen so that mechanism balancing can be implemented without the introduction of kinematical problems while the total link inertia is minimized.

Using Eq. (1) and its derivative,

$$\ddot{\mathbf{q}} = \mathbf{J}^{-1}(\dot{\mathbf{v}} - \dot{\mathbf{J}}\dot{\mathbf{q}}) \tag{5}$$

and after balancing the mechanism, the equations of motion reduce to

$$\tilde{\mathbf{M}}\dot{\mathbf{v}} + \tilde{\mathbf{V}} = (\mathbf{J}\cdot\mathbf{N})^{-T}\boldsymbol{\tau} + \mathbf{F}_T \tag{6a}$$

with

$$\tilde{\mathbf{M}} = \mathbf{J}^{T^{-1}}\mathbf{M}\mathbf{J}^{-1}, \quad \tilde{\mathbf{V}} = \mathbf{J}^{T^{-1}}\mathbf{V} - \mathbf{J}^{T^{-1}}\mathbf{M}\mathbf{J}^{-1}\dot{\mathbf{J}}\mathbf{J}^{-1}\mathbf{v} \tag{6b}$$

where $\boldsymbol{\tau}$ is the motor torque vector and $\mathbf{N}$ is a 5×5 transmission ratio matrix, see also [14]. These equations correspond to the behavior that is seen from the side of the endpoint and the endoscope. Notice that the effective mass matrix $\tilde{\mathbf{M}}$ is not constant due to the appearance of the Jacobian and the dependence of $\mathbf{M}$ to the joint variables. Although it is not possible to make $\tilde{\mathbf{M}}$ a constant matrix, its structure is simpler if the original $\mathbf{M}$ is a constant matrix. Therefore, $\mathbf{M}$ is approximately made such a matrix by proper design.

FIVE - BAR LINKAGE OPTIMIZATION

In order to optimize the five-bar linkage, see Fig. 4, we had to consider the following requirements.

1. The mechanism must have the ability to follow the path shown in Fig. 2, and similar ones.
2. The angle Ψ, that is formed by link four and the endoscope, has to be between -80° and 80° to avoid misplacement of the transmission ropes.
3. The difference $q_2 - q_1$ (Fig. 4) should be kept between 30° and 150° while the tool follows the path. This way a relatively small condition number is achieved. It is found that the mechanism condition number is minimum when $l_4 - l_2 = l_3$ and $q_2 - q_1 = 90^\circ$. The condition number increases when $l_4 - l_2 \neq l_3$ and $q_2 - q_1 \neq 90^\circ$.
4. In order to have the best possible performance during the main operation which occurs at the end of the path (point C at Fig. 2), the difference $q_2 - q_1$ at this point, should be kept between 60° and 120°. Note that the optimal difference is 90° but obviously this angle cannot be a constant.
5. The length $l_4 - l_2$ should be close to the length of l_3 (not more that $1.25l_3$), in order to minimize the condition number. At the same time, it must be long enough to allow for path following under the previous constraints. It was found that l_3 should not exceed $0.135m$ and therefore $l_4 - l_2$ must be taken between $0.135m$ and $1.25l_3 \approx 0.170m$.

The following inequalities describe the above kinematical constrains

$$30^\circ \le q_2 - q_1 \le 150^\circ \tag{7}$$

$$60^\circ \le q_{2,end} - q_{1,end} \le 120^\circ \tag{8}$$

$$l_3 \le l_4 - l_2 \le 1.25l_3 \tag{9}$$

$$-80^\circ \le \Psi \le 80^\circ \tag{10}$$

The above constraints are conflicting to some extent. For example, if one uses the length ratios that correspond to an optimal condition number, then the workspace requirements result in a larger than needed mechanism violating the minimum mass and inertia requirement.

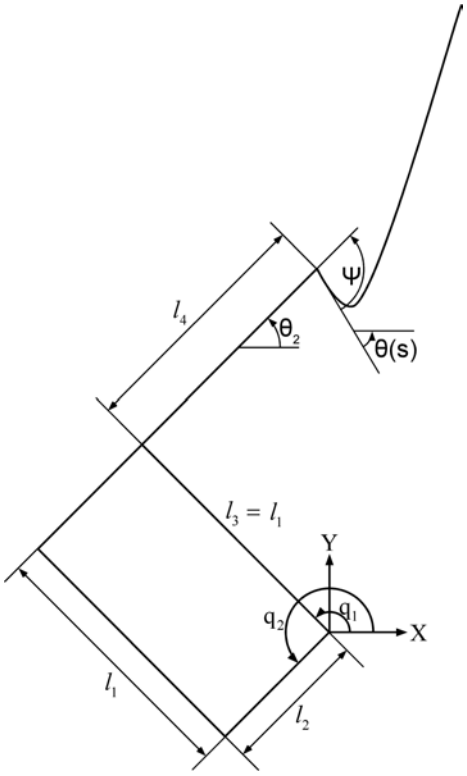

Fig. 4. Schematic view of the 5-bar linkage and the path to follow.

The above inequalities were solved in the workspace to find the optimal length of $l_4 - l_2$ and the optimal start point of the path (Fig. 2). Eq (10) and the relations $\Psi = \theta(s) - \theta_2$ and $\theta_2 = q_2 - \pi$ yield

$$-80^\circ + \theta(s) + \pi \le q_2 \le \pi + \theta(s) + 80^\circ \tag{11}$$

It is also known from the path study that $-45^\circ \le \theta(s) \le 70^\circ$ and the above inequality becomes

$$170^\circ \le q_2 \le 215^\circ \tag{12}$$

On the other hand, the five - bar linkage kinematical analysis results in the following equations

$$\begin{aligned} x_E + (l_4 - l_2)\cos(q_2) &= l_1 \cos(q_1) \\ y_E + (l_4 - l_2)\sin(q_2) &= l_1 \sin(q_1) \end{aligned} \tag{13}$$

From Eq. (13) it follows that

$$x_E \cos(q_2) + y_E \sin(q_2) = \frac{1}{2l_{4-2}}\left(l_1^2 - x_E^2 - y_E^2 - l_{4-2}^2\right) \tag{14}$$

where $l_{4-2} = l_4 - l_2$.

Setting

$$\frac{y_E}{x_E} = \frac{\sin(\omega)}{\cos(\omega)} = \tan(\omega)$$

and solving the trigonometric equation, Eq. (14), for q_2 yields

$$q_2 = \omega - Arc\cos\left(\frac{\sin(\omega)}{2l_{4-2}y_E}\left(l_1^2 - x_E^2 - y_E^2 - l_{4-2}^2\right)\right) \tag{15}$$

Using Eq. (12) and (15) and after some manipulation, the following bounds are computed

$$\begin{aligned} \omega - 170^\circ \ge Arc\cos\left(\frac{\sin(\omega)}{2l_{4-2}y_E}\left(l_1^2 - x_E^2 - y_E^2 - l_{4-2}^2\right)\right) \ge \\ \ge \omega - 215^\circ \end{aligned} \tag{16}$$

Assuming that ω is in the first quarter, Fig 5 shows the expression

$$Arc\cos\left(\frac{\sin(\omega)}{2l_{4-2}y_E}\left(l_1^2 - x_E^2 - y_E^2 - l_{4-2}^2\right)\right)$$

yields angles that are always in the gray shade area in Fig. 5, whose position changes as ω changes.

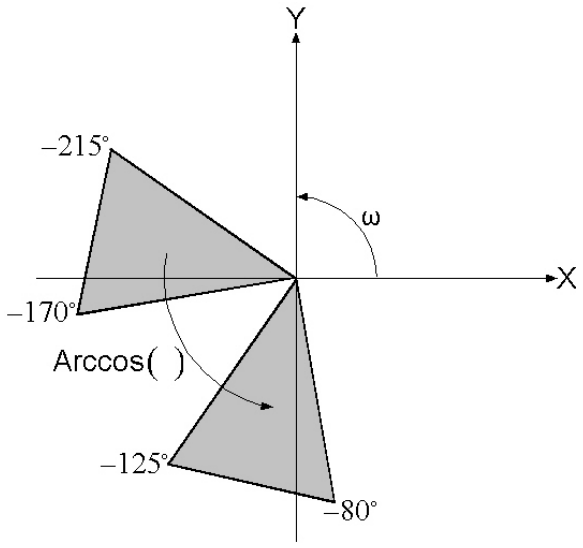

Fig. 5. The area with Arccos() in Eq. 16, whose position changes as changes.

After some transformations, Eq. (16) yields

$$\begin{aligned} l_{4-2}^2 + l_{4-2}\frac{2y\cos(\omega - 170^\circ)}{\sin(\omega)} + \left(x_E^2 + y_E^2 - l_1^2\right) \ge 0 \\ l_{4-2}^2 + l_{4-2}\frac{2y\cos(\omega - 215^\circ)}{\sin(\omega)} + \left(x_E^2 + y_E^2 - l_1^2\right) \le 0 \end{aligned} \tag{17}$$

Solving the above system of inequalities results in the required length $l_4 - l_2$. Eq. (7), (8) and (9) yield additional limits for the same expression. The computed link lengths are shown in Table 3.

Table 3. Mechanism link lengths

Link 1, l_1	13.50 cm
Link 2, l_2	7.50 cm
Link 3, l_3	13.50 cm
Link 4, $l_2 + l_4$	23.00 cm

MECHANISM IMPLEMENTATION

To minimize mechanism moving mass and inertia, the actuators must be placed on the base. In such a case, to transmit torques and read joint angles, a transmission must be employed. Among the various design options, a capstan drive and minirope type of transmission was selected. This type of transmission has the advantage of no backlash, minimum additional weight and relatively small friction levels, especially when the ropes act antagonistically.

An important problem to be solved is how to ensure that the rope lengths do not change during a *translational* motion of the spherical joint. To do this, the rope transmission path must be carefully designed. This is shown in Fig. 6. Our goal is to keep the lengths of the ropes responsible for the rotational dof constant during the translational movements of the mechanism.

Fig. 6 shows the configuration of a rope with the associated pulleys for one rotational dof. Pulleys A2 and B2 (dashed part of the rope) are hidden behind pulleys A1 and A2. The basic idea employed is described next. Assume that link 1 at its starting position is vertical. In this position the dashed part of the rope is wrapped around pulley A2 for 270° and around pulley B2 for 90°. The second part is wrapped around pulley A1 for 90° and around pulley B1 for 270°. The sum is 360° in each case.

Assume next that link 1 rotates by $q_1^1 - q_1^2$ to a new position. Following this rotation, the dashed part of the rope is wrapped around pulley A2 for $\theta_b = q_1^1 - q_1^2$. At the same time, it is unwrapped around pulley B2 by the same angle. It is obvious that the same principle is valid for the second part of the rope. Using this configuration we can keep the length of the ropes constant during any translational movement of link 1.

Another important design issue is to ensure that the rope lengths do not change during a *rotational* motion of the spherical joint. In addition, the ropes of a single rotational dof must move when one of the roll-pitch-yaw motions is in progress. It turns out that one way to achieve this requirement is to have the ropes travel on the rotation axis of the previous joint before they leave it.

Figure 7 shows a schematic view of the spherical joint design. As shown in the figure, there are three groups of pulleys, the A, B and C groups, which are responsible for rotations q_3, q_4 and q_5 respectively. Drive pulleys A_1 and A_4 rotate around the Z' axis which is fixed in the five-bar mechanism and therefore the length of the rope for joint angle q_3 is always constant.

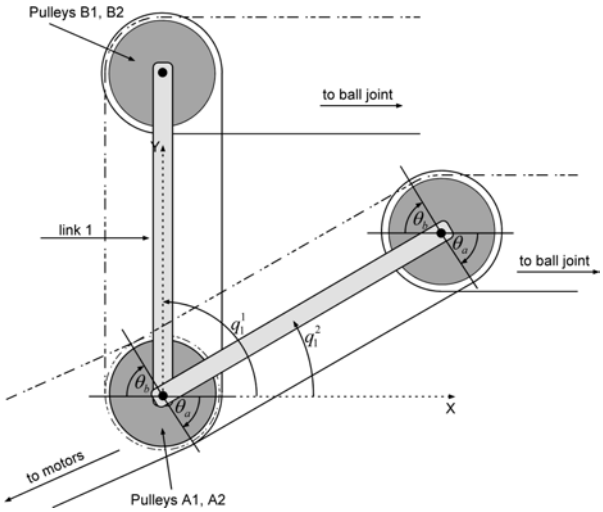

Fig. 6. Minirope transmission path design for constant rope lengths.

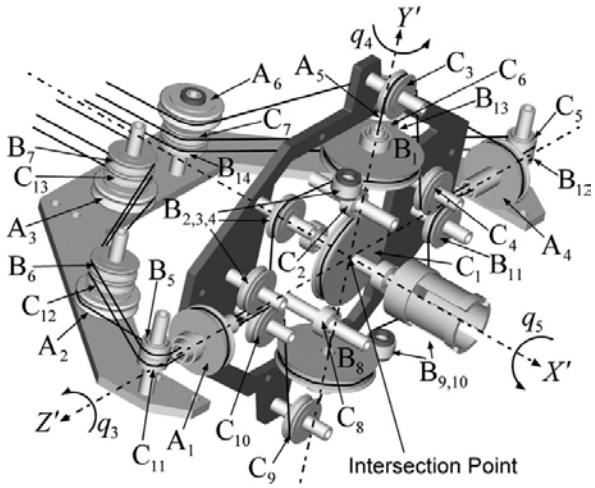

Fig. 7. Schematic view of the 3-dof spherical joint with idler pulleys and miniropes.

Idler pulleys sets B_2, B_3, B_4 and B_9, B_{10}, B_{11} receive from drive pulleys B_1 and B_8 respectively the ropes driving joint angle q_4 and guide it on the axis of rotation of the previous joint with angle q_3 and through the center of drive pulleys A_1 and A_4 to idler pulleys B_5 and B_{12}. It is also important to notice that the rope from drive pulleys B_1 and B_8 to pulleys sets B_2, B_3, B_4 and B_9, B_{10}, B_{11} is located on the plane defined by Y' and Z' axes. The rope from pulley B_5 and B_{12} to B_6, B_7 and B_{13} (not shown in Fig. 7), B_{14} respectively, is located on the plane defined by X' and Z' axes. This configuration is used in order to minimize friction between rope and pulleys and to avoid rope misplacement during pulley rotation.

Similarly, idler pulleys sets C_2, C_3, C_4 and C_8, C_9, C_{10} must guide the rope for the third joint with angle q_5 from drive

pulley C_1 through the center of drive pulleys B_1 and B_8 on the axes of the two previous joints. In such a case, motions of the two previous joints will not affect the lengths of the ropes for the last joint and roll motions will correspond to rotations of a single motor rotor. The rope from drive pulley C_1 to pulleys sets C_2, C_3, C_4 and C_8, C_9, C_{10} is located on the plane defined by Y' and Z' axes. The rope from pulley C_5 and C_{11} to C_6 (not shown in Fig. 7), C_7 and C_{12}, C_{13} respectively, is located on the plane defined by X' and Z' axes.

Figure 8 shows the assembled spherical joint design. The joint exceeds the requirements in terms of rotations and achieves rotations of $\pm 270^\circ$ about the X′-axis, $\pm 90^\circ$ about the Y′-axis and $\pm 270^\circ$ about the Z′-axis.

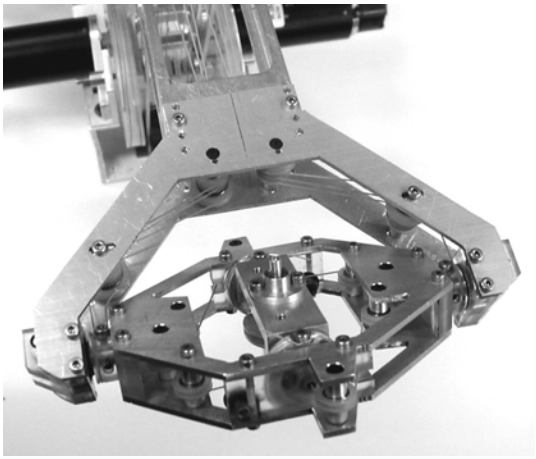

Fig. 8. The spherical joint in an assembled form.

The complete mechanism shown in Fig. 9 is constructed mostly from aluminum. However, it is designed so as to be possible to replace some of its parts with composite materials and further reduce its mass, weight and friction levels.

Capstan drives are employed for all dofs. The transmission rope is under a mild preload in order to ensure immediate response to an input torque. This preload is set equal to the dynamic load, which is the output torque divided by the radius of the output shaft. The rope diameter is chosen such that the sum of the preload and dynamic rope loads is less than 10% of the breaking strength. The minirope is made of DACRON and its diameter is approximately 0.5 mm.

Initial strain-gage based experiments showed that the friction levels are less than a tenth of a N for displacements and of the order of a few mNm for rotations. The average kinematical resolution of the mechanism is displayed in Table 4.

Table 4. Kinematical Resolution (average values)

Translational (X, Y axes)	0.05 mm
Rotational about the X' axis	0.004 rad
Rotational about the Y' axis	0.003 rad
Rotational about the Z' axis	0.003 rad

This resolution can be improved by the use of encoders with more counts per revolution than the current 500-1000 counts. Table 5 shows the computed force resolution of the mechanism.

Table 5. Force and Torque Resolution

Force (X, Y axes)	0.000270 mN
Torque about the X' axis	0.000024 mNm
Torque about the Y' axis	$9.80 \cdot 10^{-6}$ mNm
Torque about the Z' axis	$7.45 \cdot 10^{-6}$ mNm

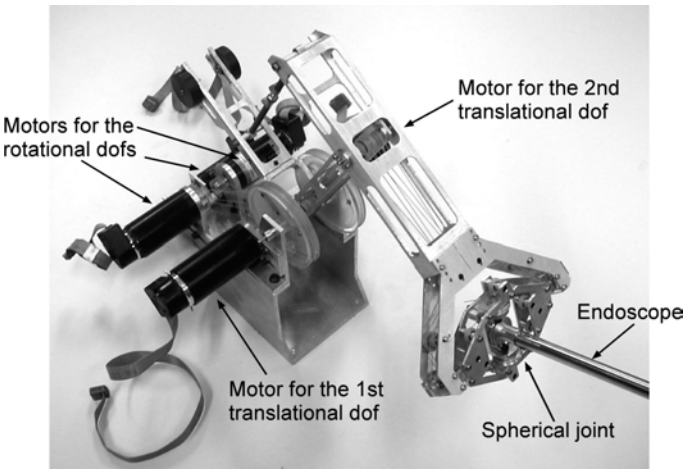

Fig. 9. The assembled 5-dof mechanism.

CONTROL

Low inertia rotating coil type DC motors actuate the device and apply torques aiming at giving the feeling that only the endoscope and the tissues are present. To compute the necessary motor currents, the equations of motion of the endoscope, see Fig. 10, are written as

$$\mathbf{M}_t \dot{\mathbf{v}}_{cm} + \mathbf{V}_t + \mathbf{G}_t = \mathbf{F} + \mathbf{F}_r \qquad (18)$$

where $\mathbf{F}$ is the vector of the applied forces and torques by the trainee on the tool, $\mathbf{M}_t$ is its mass matrix, $\mathbf{V}_t$ contains velocity terms, $\mathbf{G}_t$ contains gravity-induced terms, and $\dot{\mathbf{v}}_{cm}$ is the velocity of its center of mass. Finally, the vector $\mathbf{F}_r$ contains forces and torques which are due to tissue deformation. Since no motion is allowed in the Z direction, in the virtual environment, $\mathbf{M}_t$ is a 5×5 matrix and the rest of the vectors have appropriate dimensions.

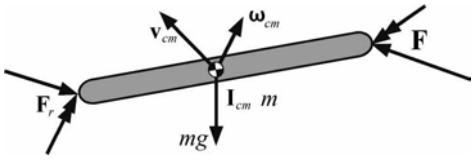

Fig. 10. Forces on the endoscope.

In general, the forces and torques $\mathbf{F}_T$ are functions of the position and velocity of the tool and are computed based on a simplified model of tissue deformation as

$$\mathbf{F}_T = \mathbf{F}_T(\dot{\mathbf{q}}, \mathbf{q}) \tag{19}$$

The currents that are sent to the motors by the power amplifiers are given by

$$\mathbf{i} = -(\mathbf{K}_\mathbf{T}\mathbf{K}_{amp})^{-1}(\mathbf{J}\cdot\mathbf{N})^T\mathbf{F}_T(\dot{\mathbf{q}}, \mathbf{q}) \tag{20}$$

where $\mathbf{K_T}$, $\mathbf{K_{amp}}$ are diagonal matrices that contain the motor torque constants and the amplifier gains, respectively.

The mechanism is now under testing and evaluation by its potential users. Preliminary results show that it meets its requirements and will prove to be a valuable tool in urological operation training.

CONCLUSIONS

A new force feedback mechanism was presented that is used in a training simulator for urological operations. The mechanism consists of a two dof, 5–bar linkage for translations and a three dof spherical joint for rotations. To be able to reproduce very small forces and moments, the mechanism has low friction, inertia and mass, is statically balanced, and has a simple mass matrix by design. To minimize the mass of its moving parts, the actuators are located at its base and forces and moments are transmitted through the use of capstan drives and idler pulleys. Roll-pitch-yaw motions of the tool result in motions of the corresponding actuator. The mechanism design and the transmission paths were described in detail. The mechanism is currently under being evaluated by its potential users.

ACKNOWLEDGMENTS

Support of this work by the PENED programs of the Hellenic General Secretariat for Research and Technology is acknowledged. The authors also wish to thank P. Hatzakos and L. Bahas for their assistance in the CAD drawings and mechanism realization.

REFERENCES

[1] Sorid, D., Moore, K. S., 2000, "The Virtual Surgeon," in IEEE Spectrum, 37, pp. 26 – 31.

[2] Chen, E., Marcus, B., 1998, "Force Feedback for Surgical Simulation," in Proceedings of the IEEE, 86, pp. 524 – 530.

[3] Goertz, R. C., 1952, "Fundamentals of General – Purpose Remote Manipulators," Nucleonics, 10, pp. 36 – 42.

[4] Salisbury, J. K., Srinivasan, A. M., 1997, "Projects in VR. Phantom – Based Haptic Interaction with Virtual Objects," IEEE Computer Graphics and Applications, pp. 6 – 10.

[5] D'Aulignac, D., Balaniuk, R., Laugier, C., 2000, "A Haptic Interface for a Virtual Exam of the Human Thigh," in Proc. IEEE Int. Conference on Robotics and Automation, pp. 2452 – 2457.

[6] Atsuko, T., Koichi, H., Toyohisa, K., 1998, "Virtual Cutting with Force Feedback," in Proceedings – Virtual Reality Annual International Symposium, pp. 71 – 75.

[7] Massie, T. H., Salisbury, J. K., 1994, "The PHANToM Haptic Interface: A Device for Probing Virtual Objects," in Proc. of the 1994 ASME Int. Mechanical Engineering Exposition and Congress, Chicago, Illinois, pp. 295 – 302.

[8] Chen, E., 1999, "Six Degree-of-Freedom Haptic System for Desktop Virtual Prototyping Applications," in Proceedings of the First International Workshop on Virtual Reality and Prototyping, pp. 97-106.

[9] Burdea, G., Patounakis, G., Popescu, V., Weiss R., 1999, "Virtual Reality – based Training for the Diagnosis of Prostate Cancer," in IEEE Transactions on Biomedical Engineering, 46, pp. 1253 – 1260.

[10] Hayward, V., Gregorio, P., Astley, O., Greenish, S., Doyon, M., Lessard, L., McDougall, J. Sinclair, I., Boelen, S., Chen, X., Demers, J - P., Poulin, J., Benguigui, I., Almey, N., Makuc, B., Zhang, X., 1998, "Freedom – 7: A High Fidelity Seven Axis Haptic Device With Application To Surgical Training," in Experimental Robotics V, Casals, A., de Almeida, A. T. (eds.), Lecture Notes in Control and Information Science 232, pp. 445 – 456.

[11] Baumann, R., Maeder, W., Glauser, D., Clavel, R., 1997, "The PantoScope: A Spherical Remote – Center – of – Motion Parallel Manipulator for Force Reflection," in Proc. IEEE Int. Conference on Robotics and Automation, pp. 718 – 723.

[12] Baur, C., Guzzoni, D., Georg, O., 1998, "Virgy, A Virtual Reality and Force Feedback Based Endoscopy Surgery Simulator," in Proceedings – Medicine Meets Virtual Reality '98, (MMVR'98), pp. 110 – 116.

[13] Kühnapfel, U., Kuhn, Ch., Hübner, M., Krumm, H.G., Maaß, H., Neisius, B., 1997, "The Karlsruhe Endoscopic Surgery Trainer as an example for Virtual Reality in Medical Education," in Minimally Invasive Therapy and Allied Technologies (MITAT), pp. 122-125, Blackwell Science Ltd.

[14] Papadopoulos, E., Vlachos K., and Mitropoulos, D., "Design of a 5-dof Haptic Simulator for Urological Operations," *Proc. IEEE International Conference on Robotics and Automation (ICRA' 02),* May 11-15, 2002, Washington, DC.